Self-Repairing Materials

DOI: 10.1002/anie.201407978

Self-Repairable Polyurethane Networks by Atmospheric Carbon Dioxide and Water**

*Ying Yang and Marek W. Urban**

Abstract: *Sugar moieties were incorporated into cross-linked polyurethane (PUR) networks in an effort to achieve self-repairing in the presence of atmospheric carbon dioxide (CO_2) and water (H_2O). When methyl-α-D-glucopyranoside (MGP) molecules are reacted with hexamethylene diisocyanate trimer (HDI) and polyethylene glycol (PEG) to form cross-linked MGP-polyurethane (PUR) networks, these materials are capable of self-repairing in air. This process requires atmospheric amounts of CO_2 and H_2O, thus resembling plant behavior of carbon fixation during the photosynthesis cycle. Molecular processes responsible for this unique self-repair process involve physical diffusion of cleaved network segments as well as the formation of carbonate and urethane linkages. Unlike plants, MGP-PUR networks require no photo-initiated reactions, and they are thus capable of repair in darkness under atmospheric conditions.*

Materials properties that extend their lifetime, thus reducing the environmental footprint, play a crucial role in today's developments of new technologies. Among particularly impressive properties of materials is their ability to self-repair.[1] Recent studies have shown that reversible breaking and reforming of dynamic covalent[2] or non-covalent bonds[3] induced by temperature, electromagnetic radiation, and/or chemical surroundings (pH, ionic strength, concentrations, and redox reactions) can be beneficial in numerous applications. However, the use of environmental gases in the self-repair of materials has never been explored. It is however well-established that plants assimilate carbon dioxide (CO_2) and water (H_2O) to produce organic compounds, thereby releasing oxygen (O_2).[4] As a result, carbohydrates are produced, and the carbon fixation cycle is one of the essential steps in this process. Can man-made materials utilize atmospheric gases to renew themselves? Notably, the use of CO_2 as a raw material to produce organic compounds has been explored, and many successful reactions of CO_2 with methanol, diols, and cyclic ethers to produce dimethyl carbonates, cyclic carbonates, and polycarbonates have been reported.[5] Furthermore, under certain catalytic conditions, CO_2 also reacts with primary or secondary amines to form urethanes and ureas.[6] Interestingly enough, when polyurethanes (PUR) are synthesized in the presence of H_2O vapors, CO_2 as well as polyurea (PUA) can be generated. The PUR networks shown in Figure 1 A are produced by reacting polyethylene glycol (PEG) and hexamethylene diisocyanate trimer (HDI), resulting in PUR and PUA segments as well as gaseous CO_2. If such a PUR network is mechanically damaged, during which C–O, C–N, and other linkages are cleaved, CO_2 and H_2O will not facilitate self-repair. However, if carbohydrates with multiple OH groups are incorporated into PURs, will CO_2 and H_2O be able to regenerate mechanically damaged network bonds? To test this hypothesis, we incorporated monosaccharides, such as methyl-α-D-glucopyranoside (MGP) containing four reactive OH groups, into cross-linking reactions of HDI and PEG. These reactions were catalyzed by dibutyltin dilaurate (DBTDL) to form MGP modified polyurethane (MGP-PUR) networks. Figure 1 B illustrates the reactions leading to MGP-PUR formation. Such networks were subjected to controllable mechanical damage.

Figure 1 C illustrates that, indeed, the MGP-PUR networks are capable of self-repair in air under ambient conditions (see the Experimental Section for details regarding MGP-PUR network preparation and damage–repair cycles). In contrast, when the same damaged MGP-PUR network is exposed to pure N_2, O_2, CO_2, or H_2O (28% RH in N_2), no self-repair occurs. The results of these experiments are illustrated in the Supporting Information, Figure S1 A–D. However, exposure to pure CO_2 at 28% RH facilitates MGP-PUR network repair (Figure 1 D). For comparison, PUR networks without cross-linked MGP (Figure 1 E) do not exhibit these unique attributes. These results clearly demonstrate that the covalent incorporation of MGP into PUR networks catalyzed by DBTDL, such as shown in Figure 1 B, facilitates self-repair under CO_2 and H_2O atmosphere. The question is then what molecular processes may govern this unique behavior, and what molecular entities are formed as a result of repair.

To identify molecular events responsible for self-repair of MGP-PUR, we followed chemical changes during the damage–repair cycle using internal reflection IR imaging (IRIRI). This analytical method, complimented by Raman spectroscopy, allows us to determine chemical changes inside scratch during the damage–repair cycle with a spatial resolution of about 1 μm^2.[7] Figure 2 A and B illustrate optical images recorded 1 min (A) and 30 min (B) after damage. Figure 2 A-1–A-5 and B-1–B-5 show the corresponding IRIRI images collected from 30×30 μm^2 area of the 1680 (A-1 and

[*] Y. Yang, Prof. M. W. Urban
Department of Materials Science and Engineering, Center for Optical Materials Science and Engineering Technologies (COMSET), Clemson University
Clemson, SC 29634 (USA)
E-mail: mareku@clemson.edu

[**] This work was supported by U.S. Army Engineering Research and Development Center (ERDC) (W7132T-09-2-0019). Partial support of the National Science Foundation under award CMMI 1332964 and J. E. Sirrine Foundation Endowment at Clemson University is also acknowledged. The authors thank Hysitron, Inc. for help with nano-indentation measurements.

Supporting information for this article is available on the WWW under http://dx.doi.org/10.1002/anie.201407978.

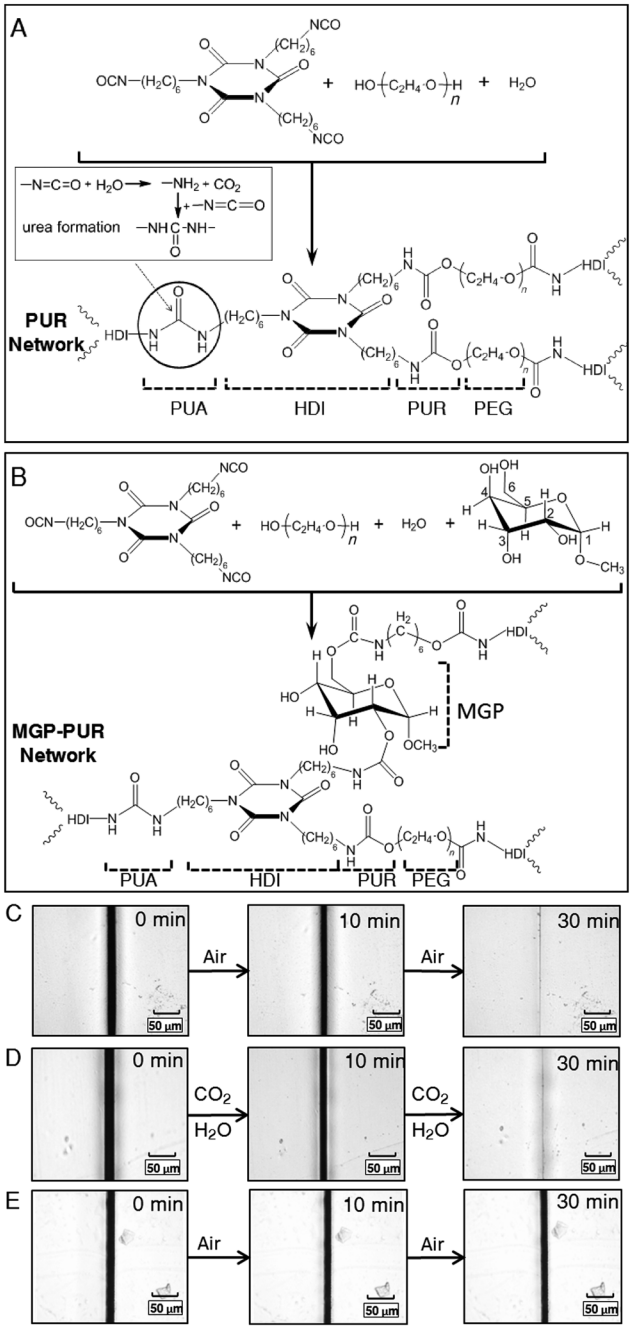

Figure 1. A) Reactions of isocyanate (NCO) groups of HDI and OH of PEG in the presence of H_2O generate CO_2 during PUR formation; B) Reactions of NCO groups of HDI and OH of PEG and MPG in the presence of H_2O result in MGP-PUR network formation. Each network linkage and/or component is identified as follows: PUA polyurea, HDI hexamethylene diisocyanate trimmer, PUR polyurethane, PEG polyethylene glycol, MGP methyl-α-D-glucopyranoside. Self-repair of MGP-PUR network exposed to: C) air at 25 °C; D) self-repair of MGP-PUR network exposed to the CO_2/H_2O mixture; E) self-repair is not observed for PUR itself exposed to air.

B-1), 1558 (A-2 and B-2), 1427 (A-3 and B-3), 1376 (A-4 and B-4), and 1045 (A-5 and B-5) cm^{-1} bands that are most sensitive to the damage–repair cycle. While *x*–*y* directions identify spatial distribution of these bands, their intensity changes (*z* direction) are also reflected in color variations (red: high; blue: low). The corresponding spectra recorded inside scratch (a/a′) and outside (b/b′) damaged area are shown in Figure 2, A′-1–A-′5 and B′-1–B′-5.

As manifested by the band intensity and color changes of IRIRI images collected 1 min after damage (Figure 2, A-1–A-5), and the corresponding IR spectra in traces A′-1–A′-5 in Figure 2, multiple bond cleavage occur upon mechanical damage. The 1680 cm^{-1} band due to H-bonded urethane C=O stretching vibrations decreases, while the 1715 cm^{-1} band due to the non-H-bonded urethanes increases (Figure 2 A-1 and A′-1), indicating the cleavage of PUR bond and dissociation of H-bonding. Furthermore, the increase of the 1620 cm^{-1} band owing to N–H deformation of primary amines (NH_2) (Figure 2 A′-1) resulting from breakage of urethane C–N and C–O bonds and subsequent hydrogen abstraction is observed. The C–O bond dissociation in PEG segments is manifested by the decrease of the 1350 cm^{-1} band (C–H deformation of ether linkages; Figure 2 A′-4). H-bonding dissociation is further substantiated by the decrease of the N–H and O–H stretching vibrations at 3346 cm^{-1} (Supporting Information, Figure S2), which overshadows spectroscopic changes that are due to hydrolysis of ether segments. Also, the bands at 1558 (Figure 2 A-2 and A′-2), 1427 (Figure 2 A-3 and A′-3), and 1376 cm^{-1} (Figure 2 A-4 and A′-4) exhibit a slight intensity increase 1 min after damage, which significantly increase during self-repair process. The increases of the 1142, 1100, and 1045 cm^{-1} bands (Figure 2 A-5 and A′-5) attributed to C–O stretching vibrations result primarily from conformational changes of HCO groups of MGP, C–O–C groups of PEG, and/or PEG/PUR C–O–C linkages. In summary, C–N and C–O covalent bond cleavage as well as urethane H-bonding dissociation are the main observed molecular evens dominating mechanical damage.

Figure 2 B illustrates the results of spectroscopic analysis after repair under atmospheric CO_2 and H_2O (28 % RH and 25 °C). The intensity decreases of the urethane C=O stretching bands at 1715 and 1680 cm^{-1} (Figure 2 B-1 and B′-1) are detected, whereas the band at 1558 cm^{-1} (Figure 2 B-2 and B′-2) increases. This is attributed to Sn chelation with C=O entities[8] of MGP during repair of MGP-PUR networks. Even though only 10^{-5} mol g^{-1} concentration levels of DBTDL were used to catalyze MGP-PUR network formation, significant increase of the bands due to DBTDL vibrations at 1558 cm^{-1} (Sn···O=C), 1376 cm^{-1} (C–H bending) (Figure 2 B-4 and B′-4), and 2856 and 2923 cm^{-1} (C–H stretching; Supporting Information, Figure S2) are detected in repaired areas. These observations are attributed to chelation and conformational changes of DBTDL during repair. We utilized energy-dispersive X-ray spectroscopy (EDX) to measure Sn concentrations inside and outside scratch. The Sn content indeed remains unchanged (Supporting Information, Figure S3). However, the concentration levels of carbon increase in the repaired area. In summary, the above data show that CO_2 and H_2O atmosphere along with MGP and DBTDL play a significant role during self-repair process. When copper(II) chloride ($CuCl_2$) was utilized as a catalyst in the same MGP-PUR networks, no self-repair was observed (Supporting Information, Figure S1 E). It should be noted that $CuCl_2$ is capable of catalyzing and

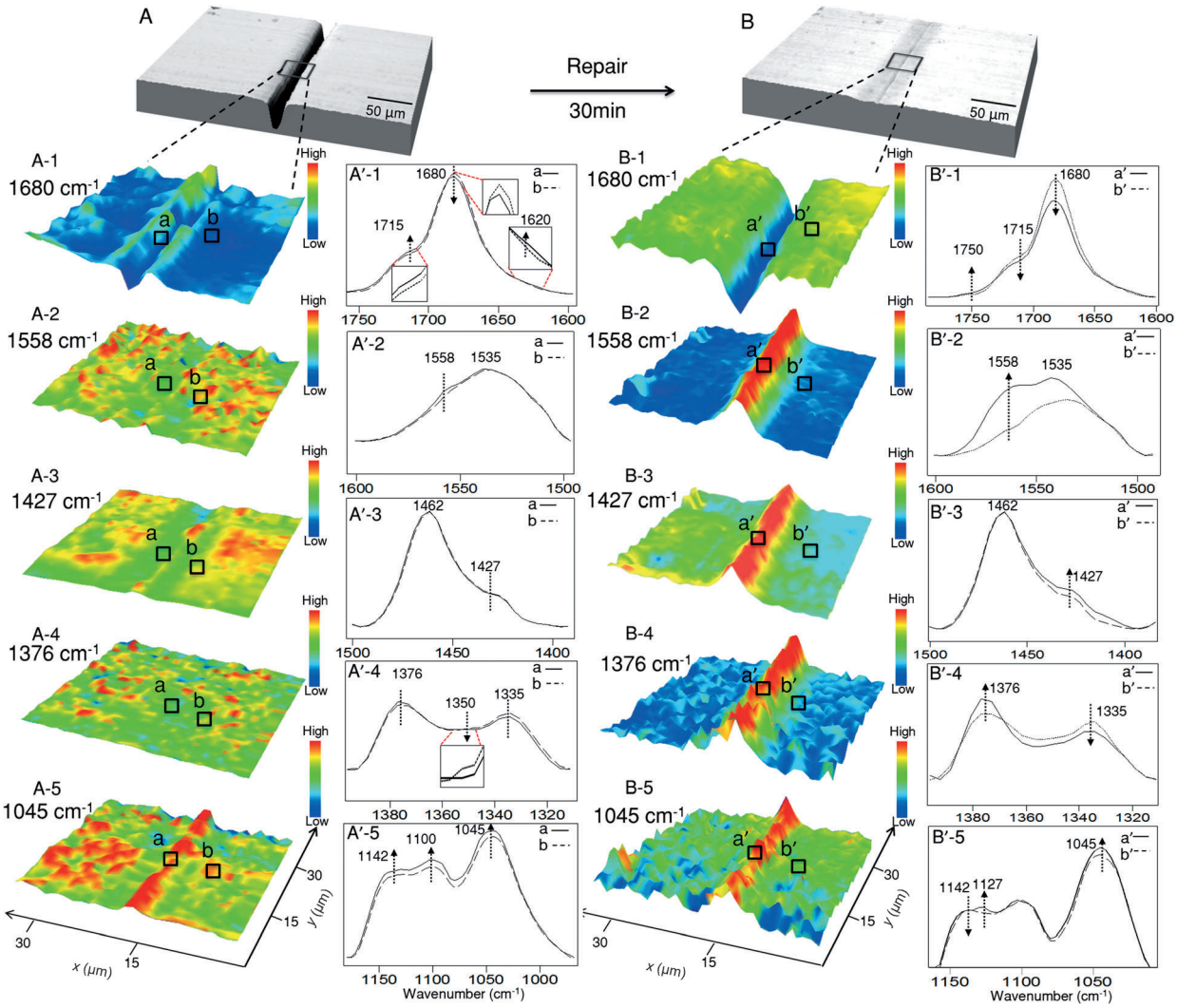

Figure 2. A) Optical image of MGP-PUR film 1 min after damage; B) optical image of MGP-PUR film self-repaired 30 min after damage. Analyzing the shades on the original 2D optical images using Envi program generated the 3D depth profiles of the optical images. Images A1 through A5 represent 3D intensity distributions of vibrational bands at 1680 (A-1), 1558 (A-2), 1427 (A-3), 1376 (A-4), and 1045 cm^{-1} (A-5) recorded from a square marked on Figure 2A. Traces A′-1 through A′-5 are IR spectra collected from areas a and b of images A-1 through A-5 respectively (a spectra collected inside scratch 1 min after damage, b spectra collected from undamaged area). Images B1 through B5 represent 3D intensity changes of vibrational bands at 1680 (B-1), 1558 (B-2), 1427 (B-3), 1376 (B-4), and 1045 cm^{-1} (B-5) recorded from a square marked on Figure 2B. Trances B′-1 through B′-5 represent IR spectra collected from areas a′ and b′ of images B-1 through B-5 (a′ spectra collected from damaged area after repair, b′ spectra collected from undamaged area).

facilitating repairs of poly(dimethylsiloxane)–poly(urethane) (PDMS-PUR) cross-linked networks.[9] Thus, only specific reactions catalyzed by DBTDL will facilitate PUR self-repair.

To verify spectroscopic changes under atmospheric CO_2 and H_2O, we conducted a series of controlled experiments in which concentrations of MGP, HDI monomer and DBTDL were varied, and interactions of individual components in the context of self-repair of MGP-PUR were examined. We reacted MGP with HDI monomer at various stoichiometric ratios, and for each MGP/HDI monomer ratio, we varied DBTDL concentration levels. ATR FTIR analysis (Supporting Information, Figure S4) showed that the degree of Sn···O=C chelation is the strongest when, on average, two OH groups of MGP are reacted with NCO. If MGP is not utilized at all, instead of Sn···O=C chelation manifested by significant increase of the 1558 cm^{-1}, this band shifts to 1565 cm^{-1} (Supporting Information, Figure S5). These results are further substantiated by the decrease of the 1335 cm^{-1} band owing to CCH deformations of the MGP ring resulting from conformational changes of the ring substituents upon chelation (Figure 2B-4 and B′-4; Supporting Information, Figure S4).[10] Considering that OH groups in C2 and C6 positions of MGP exhibit highest reactivity compared to C3 and C4 (Figure 1B), whereby C6 is greater than C2,[11] when only C6 OH react with NCO, no chelation is observed. However, when OH in C2 position is reacted, chelation with DBTDL is the strongest.

As identified in Figure 2A, dissociation of covalent bonds occurs during mechanical damage. The question is whether these bonds reform, and what structural entities result from

repair. IRIRI analysis collected on a repaired scar revealed the increase of the urethane C–N stretching band intensities at 1247 cm^{-1} along with the decrease of N–H stretching at 3346 cm^{-1} (Supporting Information, Figure S2). These changes are caused by reformation of urethane linkages. In the C–O region, the 1142 cm^{-1} band owing to OCH bending of MGP decreases, and the 1045 cm^{-1} band owing to C–O stretching vibrations continues to increase (Figure 2 B-5 and B′-5).[10] These changes result from reactions of MGP-OH with NCO groups. The same changes are detected for 1142 and 1045 cm^{-1} bands in the control experiments in which OH on MGP was reacted with NCO (Supporting Information, Figure S4). The increase of the C–H bending vibrations at 1427 cm^{-1} (Figure 2 B-3 and B′-3) that are due to asymmetric C–H deformation next to tertiary amides further substantiate these network rearrangements. Thus, reformation of C–O and C–N bonds occur as a result of substitution of the C3 and C4 OH groups of MGP. Furthermore, two new bands at 1750 (Figure 2 B′-1) and 1127 cm^{-1} (Figure 2 B′-5) that are due to C=O and C–O–C stretching, which were not observed before, are detected (Figure 2 B′-1 and B′-5). Their presence is attributed to carbonate linkage formations.[12] It should be noted that these spectroscopic changes are only detected in the presence of CO_2 and H_2O (Supporting Information, Figure S6). In summary, formations of urethane and carbonate functional linkages are primarily responsible for self-repair of MGP-PUR networks. Further spectroscopic evidence for chelation and covalent C–O and C–N bond reformation is provided by Raman analysis (Supporting Information, Figure S7). Thus, the primary event is the Sn chelation with MGP-urethane, and covalent substitution of MGP-OH moieties leading to the formation of urethane and carbonate linkages.

Mechanical properties of undamaged and repaired MGP-PUR specimens were also analyzed. MGP-PUR films were cut into two pieces. Self-repair was conducted by re-attaching two separated pieces under ambient conditions, followed by stress–strain measurements (for video footage of this process, see the Supporting Information). The results are summarized in the Supporting Information, Figure S8, which show that incorporation of MGP to form MGP-PUR networks results in the increase of the Young's modulus (E) from 3.58 for PUR to 77.7 MPa in MGP-PUR. The maximum stress of undamaged MGP-PUR is 12.97 MPa at the maximum elongation of 227 %. Upon self-repair, the maximum stress diminishes to 3.38 MPa at 48 % elongation. In another experiment, we created a scratch on a MGP-PUR film and measured storage modulus E' inside the scratch (nano-indentation) at the oscillation depth of 200 nm. During about 30 min of self-repair, the E' values inside the scratch increase from about 1.9 to about 4.5 GPa (Supporting Information, Table S2). Notably, there is an initial drop of the E' values from 1.9 to 1.1 GPa, followed by expected increase to reach about 4.5 GPa. For the undamaged MGP-PUR, the E' values are about 2.8 GPa. The initial drop of the E' values (during the first 10 min) is likely attributed to the adsorption of CO_2 and H_2O capable of plasticizing damaged network, thus enhancing segmental mobility of cleaved segments. Comparison of the stress–strain and storage moduli measurements show different rates of the recovery. The storage moduli were measured inside the scratch, whereas the stress–strain curves were obtained from bulk measurements. Under stress–strain experimental conditions, CO_2 and H_2O diffusion to the inside part of damage is limited, thus not all bonds can be reformed during the timeframe of these experiments. This is reflected in a lower maximum stress/elongation at breaking after repair. In contrast, when the scratch is created and nano-indentation experiments are performed, CO_2 and H_2O may easily diffuse into damaged areas, thus reaching full recovery of the E' values.

Supported by spectroscopic evidence discussed in Figure 2, the mechanism of MGP-PUR self-repair under atmospheric conditions is depicted in Figure 3. Figure 3 A depicts that two main molecular events that are due to mechanical damage are free radical generation and H abstraction. The proposed mechanism for self-repair is shown in Figure 3 B. Facilitated by initial coordination with H_2O, Sn complexes with MGP through chelation with the neighboring MGP-OH and urethane C=O groups to form a ring structure (a). This intermediate was spectroscopically identified as Sn···O=C chelated ring and molecular modeling shown in Figure 3 C identified that this complex during self-repair is energetically most favorable conformation. The next step involves CO_2 insertion into Sn–O bonds to form carbonate moieties (Figure 3 B b). It should be noted that the majority of CO_2 insertion reactions to Sn–O bonds are conducted under 1 atm of CO_2.[13] Reactions shown in Figure 3 occur upon MGP-urethane and Sn complexation facilitates CO_2 insertion (b) and subsequent carbonate (c) and urethane (d and e) formation. During this step, the metal carbonate moieties shown in Figure 3 B b are subject to nucleophilic attack. As shown spectroscopically, three main nucleophilic sites are present after damage: PEG-OH after cleavage of PEG C–O–C bonds, N–H moieties of urethanes, and NH_2 resulting from cleavage of urethane linkages. Reactions with PEG-OH nucleophiles result in formation of carbonate linkages (Figure 3 B c), and N–H and NH_2 groups result in the reformation of urethane linkages (Figure 3 B d and e, respectively). Although kinetics of each of these reactions remains to be determined, these reactions facilitated self-repair of MGP-PUR networks.

In summary, we developed thermosetting polyurethane networks containing cross-linked sugar moieties capable of self-repair under atmospheric conditions at ambient temperatures without intervention. By incorporating sugar moieties into polyurethanes, these materials are able to react with atmospheric CO_2 and H_2O, thus reforming covalent linkages capable of bridging cleaved network segments. Mechanical properties are recovered during self-repair process. These materials resemble behavior of plants during photosynthesis, but unlike plants, MGP-PUR networks require no photo-initiated reactions, and are thus capable of repair in the dark in air.

Experimental Section

Methyl α-D-glucopyranoside (MGP), polyethylene glycol (PEG), hexamethylene diisocyanate (HDI monomer), *N*,*N*-dimethylform-

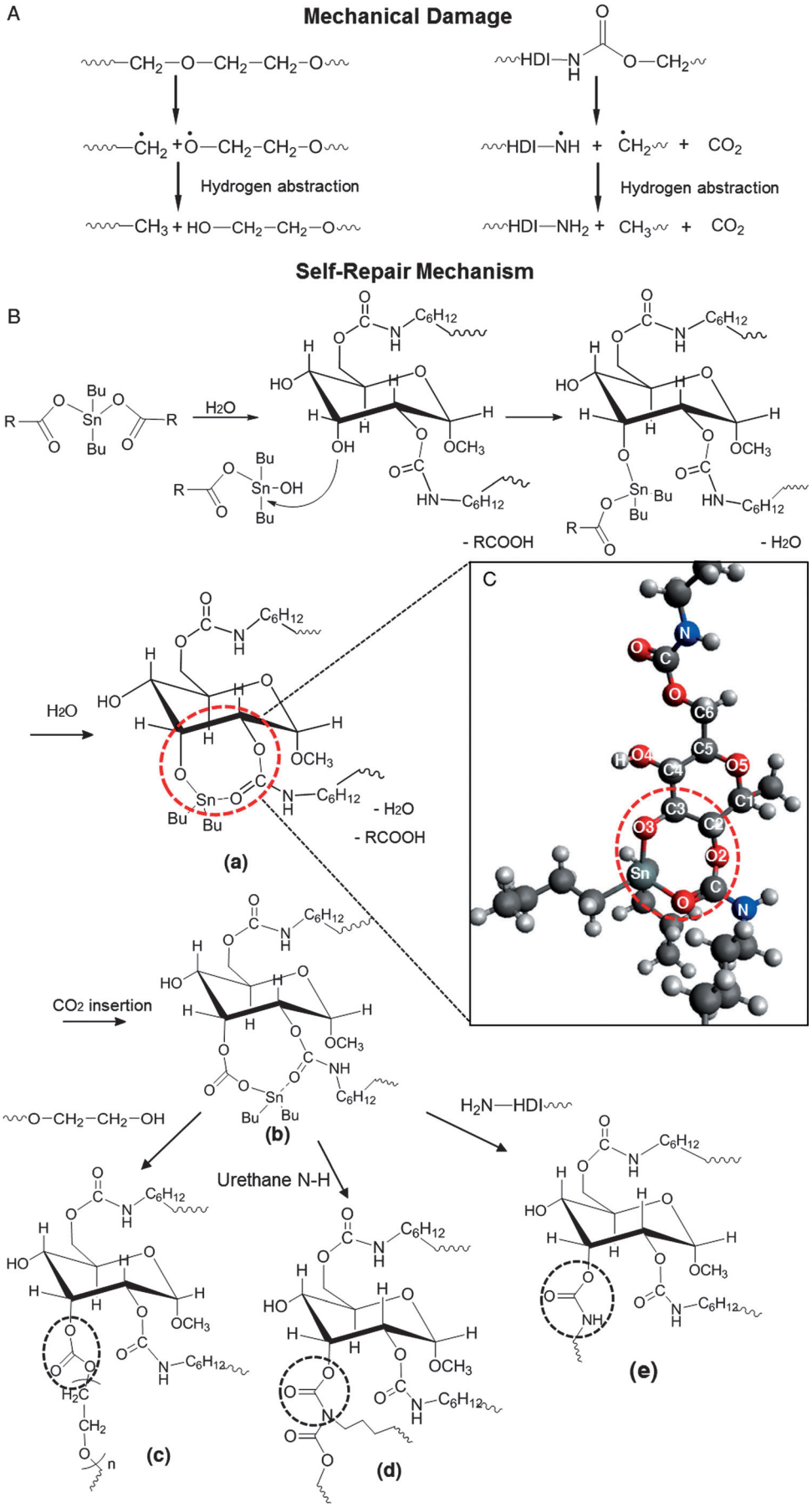

amide (DMF), dibutyltin dilaurate (DBTL), copper(II) chloride ($CuCl_2$), and magnesium chloride ($MgCl_2$) hexahydrate were purchased from Sigma Aldrich Co.; trifunctional hexamethylene diisocyanate polymer (HDI trimer) N3300a was purchased from Bayer. Carbon dioxide (CO_2) and oxygen (O_2) gases were purchased from Airgas National.

MGP-PUR films were prepared by reacting HDI trimer with MGP and PEG in DMF using overhead agitation at 500 rpm with a small four-blade polytetrafluoroethylene (PTFE) impeller in a 50 mL three-neck reaction flask at 25 °C for 10 min. MGP-PUR networks were formed by reacting HDI trimer, PEG, and MGP using stoichiometric amounts of NCO and OH groups. The molar ratio of HDI trimer/PEG/MGP = 1:0.69:0.81 were utilized while maintaining 38% (w/w) solids. This ratio was utilized to react two out of four OH groups of MGP with NCO. Such mixtures were applied to obtain an approximate film thickness of 300 μm (±4 μm) on a PTFE substrate at 75 °C and dried for 48 h.

Specimen damages were achieved by creating scratches with precisely controlled dimensions using a custom-built computerized micro-cut instrument that facilitates control of the depth, speed, and load during damage. In a typical experiment, a speed of 5 mm s^{-1} and a depth of 100 μm were utilized to obtain a 20 μm width and 100 μm deep scratches. Optical images were recorded using Leica DM2500M microscope. 3D optical images were generated by analyzing the shades of optical images using ENVI software (The Environment for Visualizing Images, Research Systems, Inc.) version 3.5. Relative humidity (RH) was controlled by utilizing enclosures containing saturated magnesium chloride solutions (RH = 28 ± 2%) and mon-

Figure 3. A) Covalent bond cleavage of MGP-PUR networks due to mechanical damage; B) proposed repair mechanism leading to carbonate and urethane formation; C) optimized molecular structure of MGP-urethane during Sn complexation that lead self-repair.

itoring RH by humidity meter (Fisher Scientific Traceable Hygrometer).

Internal reflection IR images (IRIRI) were obtained using a Cary 600 series Stingray system equipped with internal reflection IR imaging providing 1 μm spatial resolution. This system consists of a Cary 680 spectrometer, a Cary 620 FTIR microscope, an image IR focal plane array (FPA) image detector, and a germanium (Ge) imaging crystal. The IR images were collected using the following spectral acquisition parameters: under sampling ratio 2, rapid-scan speed 5 Hz, number of images per step 64, and spectral resolution 4 cm^{-1}. Image processing was performed using ENVI software (The Environment for Visualizing Images, Research Systems, Inc.) version 3.5. Traces showing IR spectra inside and outside damage were averaged over 20 spectra.

Microscopic attenuated total reflectance Fourier transform IR spectra (μATR FT-IR) were obtained using an Agilent Cary 680 FTIR single-beam spectrometer setting at 4 cm^{-1} resolution. A 2 mm diamond crystal, and maintain constant contact pressure between crystal and the film specimens was used. All spectra were corrected for spectral distortions and optical effects using the Urban–Huang algorithm.[14]

Raman spectra were recorded using a Renishaw inVia Raman microscope equipped with a computer controlled three-axis encoded (X, Y, Z) motorized stage, a RenCam CCD detector, and a Leica microscope (DM2500M). The 785 nm diode laser at 100 mW power provided an excitation source. The films were placed on the gold surface and an acquisition time of 60 s was used.

The molecular structure of the equilibrated center of chelation complexes was obtained using Avogadro software. The geometry optimization was produced under a UFF force field.

Dynamic mechanical analysis (DMA) was performed on a TA Instrument Q800 DMA. Rectangular specimens having a size of 15.73 mm × 6.09 mm × 1.07 mm were tested at a frequency of 10 Hz. Dynamic mechanical properties were measured from −100 °C up to 80 °C while heating at 2 °C min^{-1}. Dynamic moduli and mechanical damping (tanδ) were analyzed using TA Universal Analysis 2000. The measured glass transition temperature (T_g) for MGP-PUR at maximum tan δ is 54 ± 1 °C. Nano-indentation measurements were performed on Ti 950 TriboIndenter equipped with a diamond Berkovich probe. The storage modulus was measured at 220 Hz frequency, 4 μN dynamic load, and a peak force of 1000 μN. Tensile stretch test was carried out on Instron 4502 at room temperature (25 °C) at a rate of 2 mm min^{-1}. Repaired MGP-PUR for tensile stretch test was prepared by cutting and physically separating the film, followed by attachment of the separated parts together. After self-repair under ambient conditions for 30 min, the film was subject to a tensile test.

Energy-dispersive X-ray (EDX) spectra were collected on a Hitachi variable-pressure scanning electron microscope (SEM) SU6600 equipped with EDX system at a working distance of 10 mm, an accelerating voltage of 20 kV, and variable pressure mode (30 Pa). Weight % atoms of carbon (C), oxygen (O), nitrogen (N), and tin (Sn) inside and outside the scar were measured using points collection mode, and each averaged over 5 points.

Received: August 5, 2014
Revised: August 22, 2014
Published online: September 12, 2014

Keywords: carbohydrates · carbonate formation · carbon dioxide · polyurethanes · self-repairing polymers

[1] a) R. P. Wool, *Soft Matter* **2008**, *4*, 400 – 418; b) D. Y. Wu, S. Meure, D. Solomon, *Prog. Polym. Sci.* **2008**, *33*, 479 – 522; c) S. Burattini, B. W. Greenland, D. Chappell, H. M. Colquhoun, W. Hayes, *Chem. Soc. Rev.* **2010**, *39*, 1973 – 1985; d) E. B. Murphy, F. Wudl, *Prog. Polym. Sci.* **2010**, *35*, 223 – 251; e) Y. Yang, M. W. Urban, *Chem. Soc. Rev.* **2013**, *42*, 7446 – 7467.

[2] a) S. R. White, N. Sottos, P. Geubelle, J. Moore, M. R. Kessler, S. Sriram, E. Brown, S. Viswanathan, *Nature* **2001**, *409*, 794 – 797; b) X. Chen, M. A. Dam, K. Ono, A. Mal, H. Shen, S. R. Nutt, K. Sheran, F. Wudl, *Science* **2002**, *295*, 1698 – 1702; c) B. Ghosh, M. W. Urban, *Science* **2009**, *323*, 1458 – 1460; d) G. Deng, C. Tang, F. Li, H. Jiang, Y. Chen, *Macromolecules* **2010**, *43*, 1191 – 1194; e) Y. Amamoto, J. Kamada, H. Otsuka, A. Takahara, K. Matyjaszewski, *Angew. Chem.* **2011**, *123*, 1698 – 1701; f) J. Canadell, H. Goossens, B. Klumperman, *Macromolecules* **2011**, *44*, 2536 – 2541; g) C. Yuan, M. Rong, M. Zhang, Z. Zhang, Y. Yuan, *Chem. Mater.* **2011**, *23*, 5076 – 5081; K. Imato, M. Nishihara, T. Kanehara, Y. Amamoto, A. Takahara, H. Itsuka, *Angew. Chem. Int. Ed.* **2012**, *51*, 1138 – 1142; *Angew. Chem.* **2012**, *124*, 1164 – 1168; h) P. Zheng, T. J. McCarthy, *J. Am. Chem. Soc.* **2012**, *134*, 2024 – 2027; i) H. Ying, Y. Zhang, J. Cheng, *Nat. Commun.* **2014**, *5*, 3218.

[3] a) R. P. Sijbesma, F. H. Beijer, L. Brunsveld, B. J. Folmer, J. K. Hirschberg, R. F. Lange, J. K. Lowe, E. Meijer, *Science* **1997**, *278*, 1601 – 1604; b) S. J. Kalista, Jr., T. C. Ward, Z. Oyetunji, *Mech. Adv. Mater. Struct.* **2007**, *14*, 391 – 397; c) P. Cordier, F. Tournilhac, C. Soulié-Ziakovic, L. Leibler, *Nature* **2008**, *451*, 977 – 980; d) M. Burnworth, L. Tang, J. R. Kumpfer, A. J. Duncan, F. L. Beyer, G. L. Fiore, S. J. Rowan, C. Weder, *Nature* **2011**, *472*, 334 – 337; e) N. Holten-Andersen, M. J. Harrington, H. Birkedal, B. P. Lee, P. B. Messersmith, K. Y. C. Lee, J. H. Waite, *Proc. Natl. Acad. Sci. USA* **2011**, *108*, 2651 – 2655; f) M. Nakahata, Y. Takashima, H. Yamaguchi, A. Harada, *Nat. Commun.* **2011**, *2*, 511; g) Y. Chen, A. M. Kushner, G. A. Williams, Z. Guan, *Nat. Chem.* **2012**, *4*, 467 – 472.

[4] G. Edwards, D. A. Walker, *C3, C4: Mechanisms, and Cellular and Environmental Regulation, of Photosynthesis*, Blackwell Scientific Publications, New York, **1983**.

[5] a) A.-A. G. Shaikh, S. Sivaram, *Chem. Rev.* **1996**, *96*, 951 – 976; b) D. J. Darensbourg, M. W. Holtcamp, *Coord. Chem. Rev.* **1996**, *153*, 155 – 174; c) M. A. Pacheco, C. L. Marshall, *Energy Fuels* **1997**, *11*, 2 – 29.

[6] T. Sakakura, J. C. Choi, H. Yasuda, *Chem. Rev.* **2007**, *107*, 2365 – 2387.

[7] D. B. Otts, P. Zhang, M. W. Urban, *Langmuir* **2002**, *18*, 6473 – 6477.

[8] B. Renault, E. Cloutet, H. Cramail, Y. Hannachi, T. Tassaing, *J. Phys. Chem. A* **2008**, *112*, 8379 – 8386.

[9] Z. Wang, Y. Yang, R. Burtovyy, I. Luzinov, M. W. Urban, *J. Mater. Chem. A* **2014**, *2*, 15527 – 15534.

[10] M. V. Korolevich, M. R. Zhbankova, V. N. Piottukh-Peletskii, R. G. Zhbankov, *J. Struct. Chem.* **2007**, *48*, 821 – 830.

[11] Y. Kondo, *Carbohydr. Res.* **1987**, *162*, 159 – 165.

[12] J. Katon, M. Cohen, *Can. J. Chem.* **1975**, *53*, 1378 – 1386.

[13] a) T. Sakakura, Y. Saito, M. Okano, J.-C. Choi, T. Sako, *J. Org. Chem.* **1998**, *63*, 7095 – 7096; b) J.-C. Choi, T. Sakakura, T. Sako, *J. Am. Chem. Soc.* **1999**, *121*, 3793 – 3794; c) D. Ballivet-Tkatchenko, O. Douteau, S. Stutzmann, *Organometallics* **2000**, *19*, 4563 – 4567.

[14] M. W. Urban, *Vibrational spectroscopy of molecules and macromolecules on surfaces*, Wiley, New York, **1993**.

